Cancer Research

Incipient Melanoma Brain Metastases Instigate Astrogliosis and Neuroinflammation

Hila Schwartz[1], Eran Blacher[2], Malak Amer[1], Nir Livneh[1], Lilach Abramovitz[1], Anat Klein[1,3], Dikla Ben-Shushan[4], Shelly Soffer[4], Raquel Blazquez[5], Alonso Barrantes-Freer[6], Meike Müller[7], Karin Müller-Decker[7], Reuven Stein[2], Galia Tsarfaty[8], Ronit Satchi-Fainaro[4], Viktor Umansky[9], Tobias Pukrop[5,10], and Neta Erez[1]

Abstract

Malignant melanoma is the deadliest of skin cancers. Melanoma frequently metastasizes to the brain, resulting in dismal survival. Nevertheless, mechanisms that govern early metastatic growth and the interactions of disseminated metastatic cells with the brain microenvironment are largely unknown. To study the hallmarks of brain metastatic niche formation, we established a transplantable model of spontaneous melanoma brain metastasis in immunocompetent mice and developed molecular tools for quantitative detection of brain micrometastases. Here we demonstrate that micrometastases are associated with instigation of astrogliosis, neuroinflammation, and hyperpermeability of the blood–brain barrier. Furthermore, we show a functional role for astrocytes in facilitating initial growth of melanoma cells. Our findings suggest that astrogliosis, physiologically instigated as a brain tissue damage response, is hijacked by tumor cells to support metastatic growth. Studying spontaneous melanoma brain metastasis in a clinically relevant setting is the key to developing therapeutic approaches that may prevent brain metastatic relapse. *Cancer Res; 76(15); 4359–71. ©2016 AACR.*

Introduction

Malignant melanoma is the deadliest of all skin cancers. The major cause of melanoma mortality is metastasis to distant organs, frequently to the brain. Autopsy reports show that 75% of melanoma patients who died of this disease developed brain metastases, and the incidence of brain metastasis is rising (1). Brain metastases are currently incurable, and are associated with a dismal median survival of less than one year (2). Therefore, it is essential to identify factors that play a role during the earliest stages of the metastatic process that may allow preventive therapeutics following removal of the primary tumor. Dissemination of cancer cells to distant organs is a multistage process, affected by various cells in the microenvironment (3). However, while the role of the microenvironment at the primary tumor site is well documented, the crosstalk between disseminated cancer cells and stromal cells at the metastatic site are poorly characterized. Recent studies have shown that changes in the metastatic microenvironment precede the formation of macrometastases (4). Nevertheless, despite the clear clinical implications, changes in the brain microenvironment that enable the growth of metastatic melanoma cells are poorly characterized.

One of the major obstacles for molecular characterization of early metastatic niches is the lack of tractable preclinical models of spontaneous brain metastasis. Existing models of melanoma brain metastasis mostly rely on injection of tumor cells via an intracardiac or intracarotid route, resulting in rapidly forming experimental macrometastases (2, 5). While these models were instrumental in contributing to our understanding of advanced stage metastatic disease, they do not allow comprehensive studies of the multi-stage process of metastasis. Additional models were developed by injection of patient-derived melanoma cell lines, giving rise to spontaneous brain metastases in immunodeficient mice (6, 7). Transgenic models of melanoma (8–12) are valuable for studying primary tumor initiation and progression. However, they encompass infrequent brain metastases with very long latency and thus preclude systematic analyses of the early changes in the brain microenvironment that enable metastatic growth (13).

To overcome this challenge, we established and characterized a transplantable mouse model system of spontaneous melanoma brain metastasis following orthotropic inoculation of

[1]Department of Pathology, Sackler School of Medicine, Tel Aviv University, Tel Aviv, Israel. [2]Department of Neurobiology, George S. Wise Faculty of Life Sciences, Tel Aviv University, Tel Aviv, Israel. [3]Department of Cell Research and Immunology, George S. Wise Faculty of Life Sciences, Tel Aviv University, Tel Aviv, Israel. [4]Department of Physiology and Pharmacology, Sackler School of Medicine, Tel Aviv University, Tel Aviv, Israel. [5]Department of Internal Medicine III, Hematology and Medical Oncology, University Hospital Regensburg, Regensburg, Germany. [6]Institute of Neuropathology, University Medical Center Göttingen, Göttingen, Germany. [7]Tumor Models Unit, German Cancer Research Center, Heidelberg, Germany. [8]Department of Diagnostic Imaging, Chaim Sheba Medical Center, Ramat Gan, Israel. [9]Skin Cancer Unit, German Cancer Research Center (DKFZ), Heidelberg and Department of Dermatology, Venereology and Allergology, University Medical Center Mannheim, Ruprecht-Karl University of Heidelberg, Mannheim, Germany. [10]Department of Hematology/Medical Oncology, University Medical Center Göttingen, Göttingen, Germany.

Note: Supplementary data for this article are available at Cancer Research Online (http://cancerres.aacrjournals.org/).

This work was performed in partial fulfillment of the requirements for a Ph.D. degree by Hila Schwartz, Sackler School of Medicine, Tel Aviv University.

Corresponding Author: Neta Erez, Department of Pathology, Sackler School of Medicine, Tel Aviv University, Tel Aviv 69978, Israel. Phone: 972-3640-8689; Fax: 972-3640-9141; E-mail: netaerez@post.tau.ac.il

doi: 10.1158/0008-5472.CAN-16-0485

melanoma-derived cell line in immunocompetent mice. We chose the Ret-melanoma model (12). Importantly, the *RET* oncogene is mutated in human melanoma (14, 15), particularly in desmoplastic melanoma, which has an increased risk for brain metastasis (16). While mutations in the RET oncogene are not very frequent in human melanoma, they result in activation of common oncogenic downstream signaling pathways, such as MEK kinases and p38 MAPK (12). In addition, Ret-melanoma cells express typical melanoma antigenic markers including TRP2, gp100 and TRP1 (17). The transplantable model we established recapitulates the pathologic multistep process of metastasis, including a relatively high penetrance of brain macrometastases.

We characterized the formation course of micro- and macrometastases and established molecular tools by which metastases can be quantitatively assessed. Moreover, we show that brain micrometastases can be detected intravitally by quantitative analysis of melanoma-derived transcripts in peripheral blood and in cerebrospinal fluid (CSF).

Astrocytes play a principal role in the repair and scarring process of the brain following injuries. Dysregulation of their function contributes to the pathogenesis of several diseases, including neurodegenerative disorders (18), brain cancer, and metastasis (19). Reactive astrogliosis is the primary response of astrocytes to brain insult, characterized by proliferation, migration to the injured site, and extensive upregulation of glial fibrillary acidic protein (GFAP) (20). We and others have previously shown that activated astrocytes surround and infiltrate experimental brain metastases (21–23). However, the role of astrocytes in facilitating the formation of spontaneous brain metastases is largely unknown. We therefore utilized our spontaneous model to characterize early changes in the brain microenvironment, and the role of astrocytes in promoting incipient growth of melanoma cells. Here we demonstrate early changes in the brain microenvironment that precede the formation of spontaneous brain metastases, including breakdown of the blood–brain barrier (BBB) and vascular hyperpermeability. Moreover, we show activation of astrogliosis and neuroinflammation in incipient brain metastases, and that astrocytes are activated by paracrine signaling from melanoma cells to express a gene signature associated with brain tissue damage. Finally, we demonstrate a functional role for astrocytes in facilitating the initial growth of melanoma cells in the brain. Thus, our approach for systematic detection of micrometastases in a clinically relevant mouse model provides a platform to study the early interactions between metastatic tumor cells and stromal cells in the brain microenvironment that regulate metastatic growth.

Materials and Methods

Ethical statement

Mice were maintained at the SPF facilities of the Tel Aviv University and the Center for Preclinical Research at the German Cancer Research Center, Heidelberg. All experiments involving animals were approved by the TAU Institutional Animal Care and Use Committee (approval # M-13-078) or by the local regulatory authorities in Karlsruhe, Germany (license No. G116/13). Five- to 8-week-old male C57BL/6 (Harlan) or female C57BL/6 (Charles River Laboratories) mice were used. Use of human samples was approved by the Institutional Review Board Committee at the University Medical Center, Göttingen, Germany.

Orthotropic inoculation

A total of 5×10^5 low passage (< p15) Ret-melanoma sorted (RMS) cells were resuspended in PBS and mixed 1:1 with growth factor–reduced Matrigel (356231, BD Biosciences) to a final volume of 50 μL. Mice were anesthetized by isoflurane, and injected subdermally at the right dorsal side, rostral to the flank, with a 29G insulin syringe (BD Biosciences).

Tumors were measured 4 times weekly by calipers. Tumor volumes were calculated using the formula $X^2 \times Y \times 0.5$ (X-smaller diameter, Y-larger diameter).

Tumor excision

Mice were anesthetized with ketamine (100 mg/kg) xylazine (10 mg/kg). An incision was made in the skin medial to the tumor. Tumors were detached from inner skin with clean margins to prevent recurrence. Next, tumor-associated connective tissue and blood vessels were detached. The incision was sutured using vicryl threads (J304H, ETHICON). Mice were weighed weekly and monitored until relapse.

Tissue collection

Mice were anaesthetized with ketamine/xylazine, heart-perfused with PBS and brains, lungs, and livers were harvested. Brains were macroscopically examined for abnormal lesions and cut mid-sagittaly. Right hemispheres were taken to histology, and left hemispheres were flash-frozen in liquid nitrogen.

Ex vivo modeling of micrometastases

Normal brains were harvested and cut mid-sagittaly. Serial dilutions of RMS cells (10^2–10^6) were added to M-tubes (Miltenyi Biotec) and homogenized with the hemispheres.

Cerebrospinal fluid analysis

Three to 5 μL cerebrospinal fluid (CSF) samples were obtained as described previously (24) with the following modifications: Hirschmann Micropipettes capillaries (Z611239, Sigma) were pulled at 63.5°C with a pipette puller (CP-10, NARISHIGE). The sharp edge of the pulled capillary was cut open. Mice were anesthetized with ketamine/xylazine, placed in Kopf Stereotaxic Alignment System, and CSF was collected from the cisterna magna. Capillaries were gently removed and placed on a 25G needle attached to a 1-mL syringe, in which the plunger was prepulled. The attachment point was sealed (to ensure outflow only), the CSF was slowly released and samples were stored at −80°C. Only blood-free samples were analyzed.

For gene expression analysis, samples were thawed on ice, and direct reverse transcription was next performed without RNA purification step (K1671, MAXIMA-RT kit, Life Technologies). CSF from normal mice was used as negative control, and purified exosomes from RMS cells as positive controls (ExoQuick-TC kit, EXOTC10A-1, SBI). cDNA was diluted 1:2 and qPCR was performed (StepOne, Applied Biosystems). CSF samples from spontaneous metastases were further amplified with additional 40 cycles of PCR (C1000, Bio-Rad). Two microliters of PCR products were run on 2% agarose gels.

Statistical analysis

Data were analyzed with Student's t test. Correlation analyses were performed with Fisher exact test (2×2 contingency table). Data were considered significant when $P < 0.05$. All statistical tests were two-tailed.

Results

An immunocompetent mouse model of spontaneous melanoma brain metastasis

One of the main challenges in studying brain metastasis is the lack of murine models that fully recapitulate invasion, migration, and distant organ colonization by tumor cells (11). We therefore set out to establish a model of spontaneous melanoma brain metastasis that will incorporate all steps of metastatic disease in immunocompetent mice. To that end, we utilized a transplantable melanoma cell line derived from a spontaneously occurring skin tumor in *Ret* transgenic mice (25). To facilitate the detection of metastasizing melanoma cells *in vivo*, we engineered the Ret-melanoma cells to express the fluorescent reporter gene mCherry and selected for highly fluorescent cells by FACS. Transduced Ret cells will be referred to hereafter as Ret-mCherry Sorted cells (RMS). Importantly, expression of mCherry did not affect proliferation rates as compared with the parental cell line (data not shown). A total of 5×10^5 RMS cells were inoculated orthotopically by subdermal injection (previously demonstrated to be preferential for spontaneous metastasis; ref. 26) into syngeneic mice, and primary tumor growth was analyzed (Fig. 1A and B). Notably, the formation of aggressive local tumors suggested that the expression of mCherry did not induce an immunologic host response. To adequately represent the clinical settings, local tumors were surgically excised and mice were monitored for brain metastases. When analyzing injected mice that did not succumb to pulmonary metastases, 50% of the remaining injected mice developed brain macrometastases approximately 3–6 months after primary tumor removal (Supplementary Table S1). The overall incidence of brain macrometastases was 23% ($n = 60$). Brain macrometastases were detected intravitally by MRI imaging (Fig. 1C; Supplementary Fig. S1), or visualized by *ex vivo* fluorescent imaging of mCherry-positive foci (Fig. 1D), and by macroscopic examination (Fig. 1E). The calculated average volume of macrometastases by MRI was 2 mm^3 (Supplementary Fig. S1). The presence of mCherry-expressing cells in brains of injected mice was confirmed by FACS analysis. mCherry-positive cells represented a distinct population, which consisted of 5%–9% of total cells in the brain (Fig. 1F). Histology and immunostaining of tissue sections from various regions of brain lesions further validated the presence of parenchymal macrometastases (Fig. 1G–K and Supplementary Fig. S1). Moreover, the pattern of brain metastases in mice (as reflected by the analysis of MRI and histology) resembled meningeal spread, characteristic of human metastatic disease, which represents a devastating complication of brain metastases (27).

Quantitative molecular detection of micrometastases

Macrometastases are the final stage of a long complex process. To gain insight on the initial steps of metastasis, we analyzed the formation of brain micrometastases in this model. We first evaluated whether the expression of mCherry can be quantitatively assessed as a reporter for the presence of micrometastases. Expression analysis of RNA from local tumors confirmed the expression of mCherry *in vivo* (Supplementary Fig. S2A). We next tested whether quantitative detection of mCherry could be utilized to determine brain metastatic load. To that end, we established an *ex vivo* modeling system of micrometastases by mixing known numbers of RMS cells with normal brains followed by combined homogenization and RNA extraction (Fig. 2A). qPCR analysis of mCherry revealed a linear correlation between melanoma cell numbers and mCherry expression ($r^2 = 0.98$; Fig. 2B). The same linearity was obtained for the known melanoma markers *Trp-1*, *Trp-2* ($r^2 = 0.99$; Fig. 2C and D), *Mart-1* and *Mitf-v2* (not shown), confirming that this *ex vivo* calibration system can be used to quantify the number of melanoma cells. Strikingly, quantification of melanoma cells in brains of mice with no detectable macrometastases revealed mCherry-positive signal equivalent to as few as 100 cells (Fig. 2E and F). Notably, mice were heart perfused to ascertain that the mCherry signal did not originate in circulating melanoma cells, but rather from parenchymal metastases. Thus, this molecular quantification system provides a reliable tool to identify incipient metastatic lesions and to study the earliest stages of metastatic disease.

Utilizing this molecular detection system, we next quantified the percentage of micrometastases. Analysis of brains from 40 injected mice revealed that one month after primary tumor removal, 40%–50% of the mice had micrometastases composed of $<10^4$ cells (Fig. 2E and F). Similarly, we quantified micrometastases in other organs (Supplementary Table S2; Supplementary Fig. S2B and S2C). In addition, micrometastases were detected and quantified by FACS analysis. Micrometastases consisting of less than 10^4 cells corresponded to a population of approximately 1%–1.5% mCherry-positive cells of total brain cells (Fig. 2G and H and Supplementary Fig. S3).

We next asked whether metastases formation in this model is a continuous process. To that end, we averaged the relative expression signal from mCherry-positive brains at different micrometastases endpoints: 7, 14, and 56 days after subdermal inoculation. Analysis indicated that the mCherry signal increased exponentially with time in three independent cohorts analyzed (Fig. 2I). These results indicate that micrometastases are proliferative; or alternatively, that additional micrometastatic lesions form with disease progression. To obtain spatial insight of micrometastases, we utilized mCherry detection to analyze the histopathology of brain micrometastases. Analysis of staining revealed that disseminated cells were located in the choroid plexus and in the brain parenchyma (Fig. 2J and K and Supplementary Fig. S2D–S2K). To test whether micrometastases detected by qPCR correlate with the histologic findings, we examined the corresponding hemispheres by qPCR, as above. We found a significant correlation between the presence of melanoma cells in brain sections and their detection by qPCR in the contralateral hemisphere, thus enabling efficient and accurate screening for micrometastases-bearing brains (Fig. 2L).

Intravital diagnosis of brain metastases by CSF analysis

Seeking to extend the clinical relevance of micrometastases detection, we next tested the feasibility of intravital analysis and monitoring of micrometastases. To that end, we initially analyzed peripheral blood from injected mice. Calibration curves for mCherry and *Trp-2* detection by qPCR were analyzed by mixing ("spiking") known amounts of RMS cells with 15 μL samples of normal peripheral blood (Supplementary Fig. S4A and S4B). We found that circulating melanoma cells could be readily detected and quantified. Moreover, there was a significant correlation between the presence of melanoma cells in blood and brain metastases (Supplementary Fig. S4D). Interestingly, the signal was much higher in blood than in brain and corresponded to an average of 60 cells/μL (Supplementary Fig. S4C), reflecting the

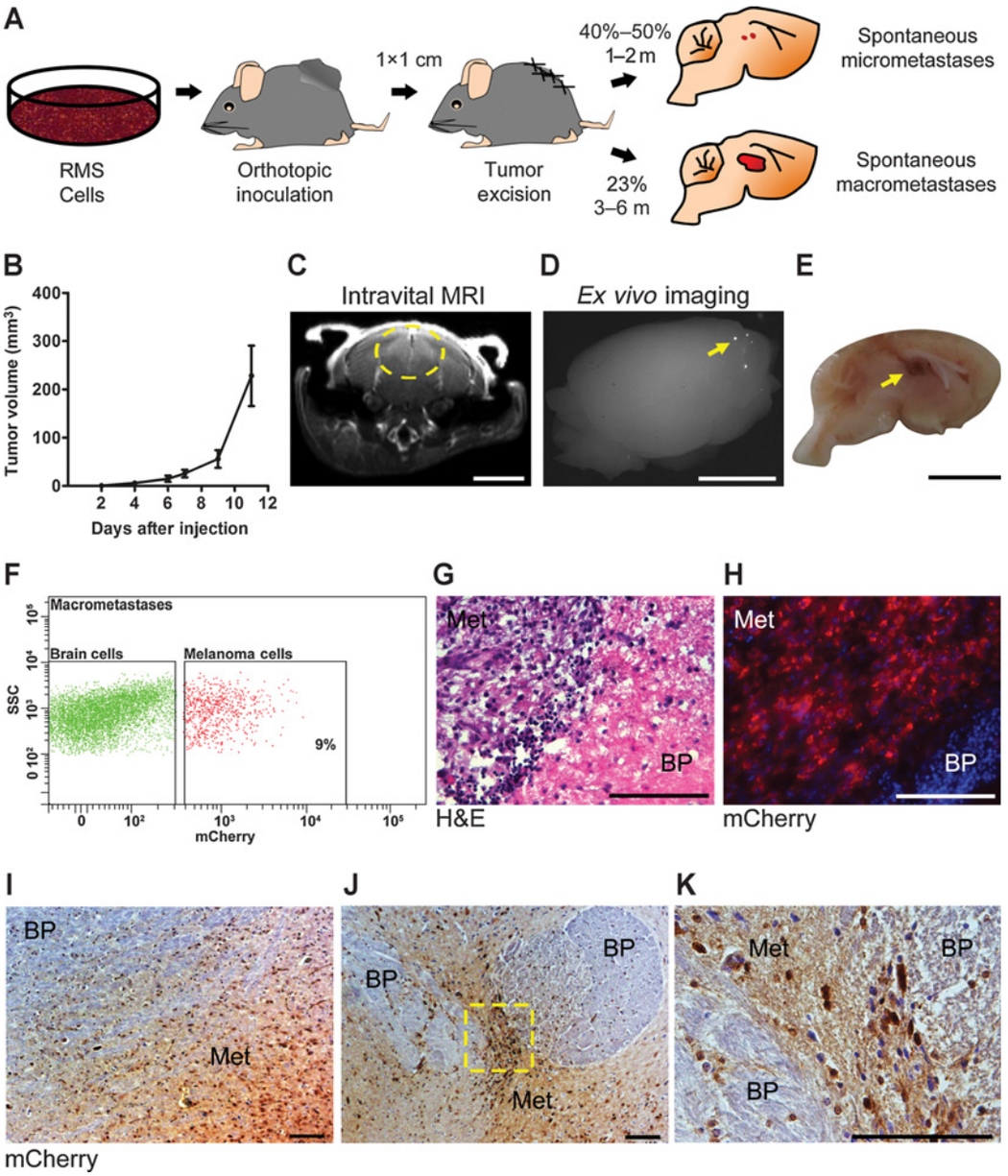

Figure 1.

A spontaneous mouse model of melanoma brain metastasis. **A,** illustration of the model. **B,** local tumor growth kinetics of Ret-melanoma cells. Representative growth curve of five different cohorts, $n = 60$. Error bars, SEM. **C–K,** brain macrometastases were quantified in mice that did not die of extracranial metastases 3–6 months after primary tumor removal ($n = 14/60$). Macrometastases were detected by MRI or fluorescent imaging, gross examination, and either FACS or histology analyses. **C,** MRI image of spontaneous brain macrometastases. Scale bar, 5 mm; $n = 8$. Dashed circle, metastatic lesion. **D,** fluorescent *ex vivo* imaging of brains with macrometastases. $n = 6$; scale bar, 5 mm. **E,** gross anatomical view of a brain with spontaneous macrometastases 3 months after primary tumor excision. $n = 3$; scale bar, 5 mm. **F,** FACS analysis of brain single-cell suspensions from injected mice, $n = 3$. **G,** H&E staining of brain bearing macrometastases. **H,** fluorescent imaging of mCherry-expressing melanoma cells. Nuclei were stained with DAPI. **I–K,** IHC for mCherry in brains with macrometastases. **K** is a magnification of **J**. **G–K** are representative pictures of multiple panels analyzed in 3 mice. Scale bars, 100 μm. Additional images are in Supplementary Fig. S1.

abundance of circulating melanoma cells, only part of which will eventually colonize the brain.

As circulating tumor cells probably indicate the presence of metastases in other organs in addition to the brain and are therefore not an unequivocal predictor of brain micrometastases, we further analyzed samples of CSF. We initially audited the presence of melanoma-derived transcripts in 3-μL CSF isolated from mice bearing experimental brain macrometastases (intracardiac or intracranial injections). Analysis by qPCR revealed expression of mCherry and the melanoma transcripts *Trp-2* and

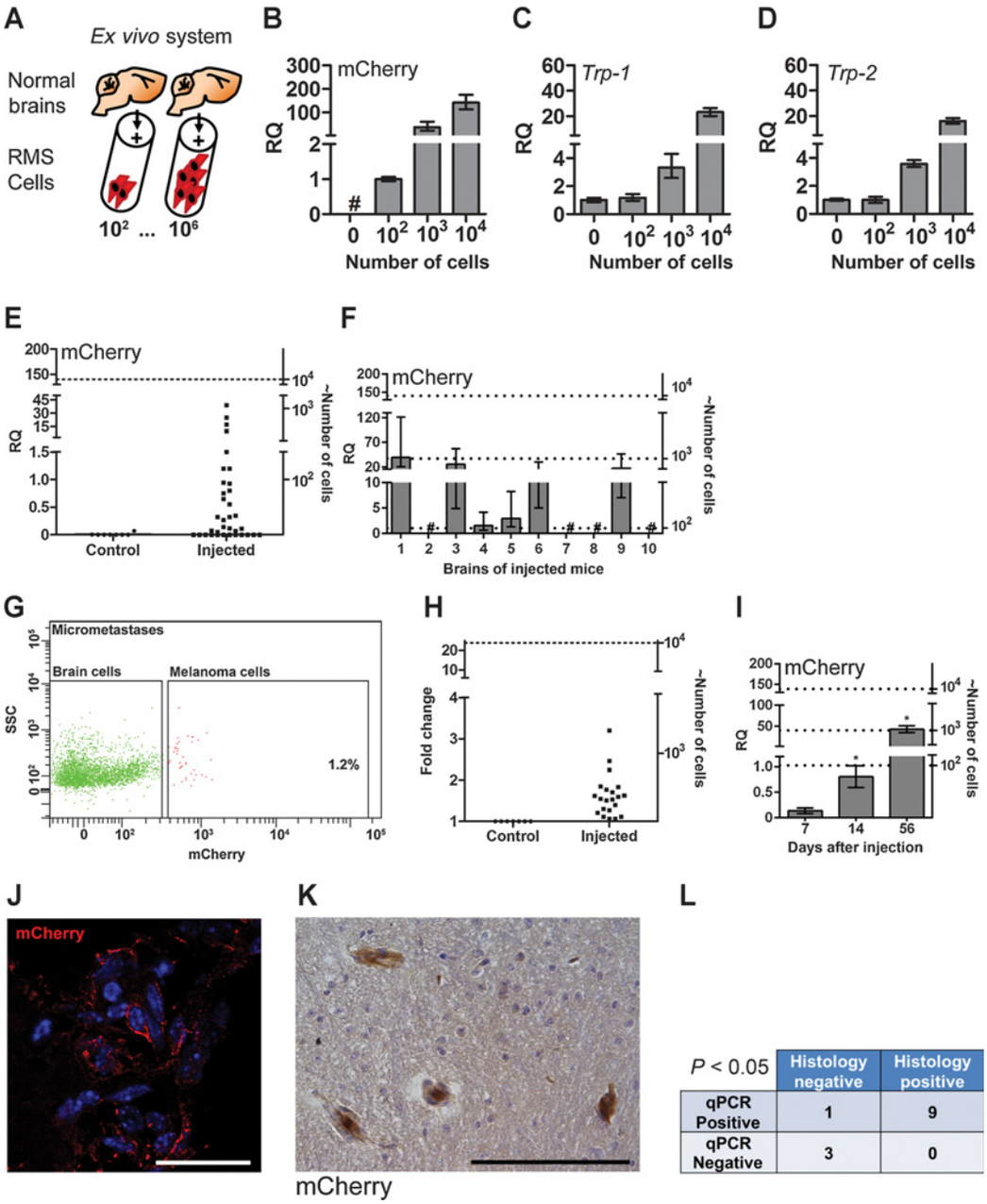

Figure 2.

Detection and molecular quantification of brain micrometastases. **A,** schematic diagram of *ex vivo* micrometastases quantification. **B–D,** quantitative calibration of metastatic load detection. qPCR results for mCherry (**B**), *Trp-1* (**C**), and *Trp-2* (**D**) in known numbers of cells, as shown in **A**. Representative results of three independent experiments. In all qPCR analyses, results were normalized to *Hprt* and to the signal of 10^2 cells. Error bars represent RQ min and max of technical repeats. #, undetected expression. **E,** qPCR analysis of mCherry expression and metastatic load one month after primary tumor excision in injected mice ($n = 40$) or control mice ($n = 8$). **F,** metastatic load in a cohort of injected mice ($n = 10$). **G,** FACS analysis of micrometastases-bearing mouse. Representative plot from four independent cohorts analyzed ($n = 21$). **H,** summary of injected mice analyzed by FACS for metastatic load, as in **G**. Left *y*-axis, fold change in number of detected mCherry$^+$ cells per 10,000 events, normalized to control mice ($n = 7$). Right *y*-axis, approximate number of cells derived from the calibration curve presented in Supplementary Fig. S3C. **I,** qPCR of mCherry expression at different time points following tumor cell injection, as indicated. Each time point represents the average expression in separate cohorts; $n = 4$, 3, 4, respectively. Error bars, SEM. *, $P < 0.05$ (Student *t* test). **J–K,** fluorescent (**J**) and IHC (**K**) staining in brain tissue sections. Representative images from multiple fields analyzed in 6 mice. In **J,** scale bar, 25 μm; **K,** 100 μm. Additional images in Supplementary Fig. S2. **L,** correlation of qPCR with histology analyses of injected mouse brains; $n = 13$ (Fisher exact test).

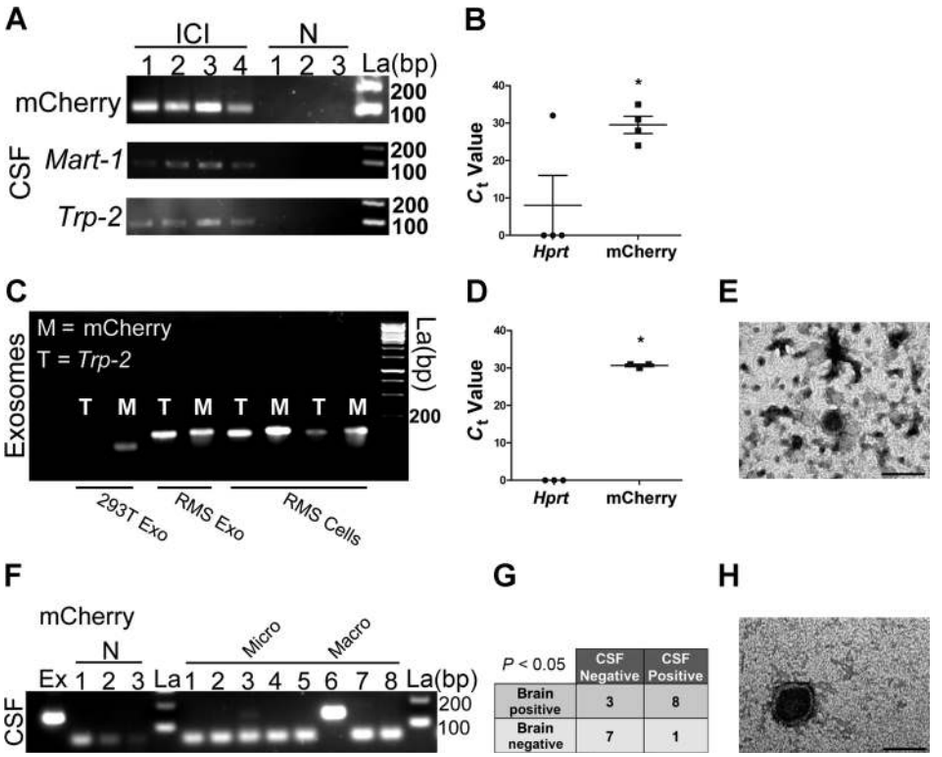

Figure 3.

Intravital detection of melanoma-derived transcripts in CSF. **A,** gel electrophoresis of mCherry, *Trp-2*, and *Mart-1* qPCR products in CSF isolated from mice with macrometastases, 10 days after intracranial injections (ICI, $n = 4$), or from normal mice (N, $n = 3$). **B,** C_t values of *Hprt* and mCherry from qPCR analysis described in **A**. *, $P < 0.05$ (Student t test). **C,** gel electrophoresis of mCherry and *Trp-2* PCR products in RMS cells or RMS-derived exosomes. Exosomes isolated from 293T cells were used as negative control. Results are representative of two independent experiments. **D,** C_t values of *Hprt* and mCherry from PCR analysis of RMS exosomes as described in **C**. **, $P < 0.01$ (Student t test). **E,** TEM image of exosomes isolated from RMS-conditioned medium (RMS-CM). Scale bar, 200 nm. **F,** gel electrophoresis of mCherry qPCR products in CSF isolated from mice with spontaneous brain micro- and macrometastases, 3 months after tumor excision, $n = 8$. Control CSF was isolated from normal mice (N, $n = 3$). **G,** correlation between mCherry detection in CSF and brain, $n = 19$ (Fisher exact test). **H,** TEM image of exosomes isolated from CSF from mice bearing spontaneous melanoma brain metastases. Scale bar, 100 nm. La, ladder; bp, base pairs; Ex, positive control, exosomes isolated from RMS-CM.

Mart-1 (Fig. 3A and Supplementary Fig. S5). Notably, expression of the housekeeping genes *Hprt* (Fig. 3B) and *Gus* (not shown) was undetermined, and no mCherry-containing cells could be detected (Supplementary Fig. S5), suggesting that melanoma-derived transcripts may be located in vesicles secreted by metastatic cells into the CSF (e.g., exosomes or melanosomes). This hypothesis is further supported by the observation that mCherry and *Trp-2* were detected in exosomes isolated from RMS cells *in vitro*, while the expression of *Hprt* was undetermined (Fig. 3C and D). Detection of vesicles in the range of 30–100 nm by transmission electron microscopy (TEM) confirmed the presence of exosomes (Fig. 3E and Supplementary Fig. S5). Encouraged by these results, we tested whether CSF analysis could be utilized as a diagnostic tool for detection of spontaneous brain metastases. Analysis of CSF from subdermally injected mice confirmed the presence of mCherry transcripts. Furthermore, the signal intensity corresponded to metastatic load, with stronger signals in mice with macrometastases (Fig. 3F). Importantly, there was a significant correlation between detection of melanoma transcripts in CSF and metastases in the corresponding brains (Fig. 3G). Imaging by TEM confirmed the presence of exosomes in CSF of mice bearing spontaneous brain macrometastases (Fig. 3H). Thus, brain micrometastases can be detected intravitally, providing a system to study the earliest stages of metastases formation.

Brain micrometastases are associated with vascular hyperpermability

Tumor vasculatures are known to be pathologically hyperpermeable in advanced tumor lesions (28, 29). However, very little is known about changes in the permeability of blood vessels in micrometastases. To test whether vessel hyperpermeability is a feature of brain micrometastases, we performed a modified Miles assay. Brains of injected mice analyzed were free of macrometastases, as confirmed by *ex vivo* fluorescent imaging and qPCR analysis of mCherry expression (Supplementary Fig. S6). Analysis of Evans blue extravasation into brain tissue revealed that spontaneous formation of brain micrometastases was associated with increased vascular hyperpermeability (Fig. 4A). To further quantify the leakiness of brain blood vessels and the integrity of the blood–brain barrier (BBB), mice were injected with FITC-Dextran (70 kDa). Quantification of staining indicated that mice with micrometastases had significantly more leaky vessels than control mice (Fig. 4B–E). Furthermore, staining of melanoma cells in

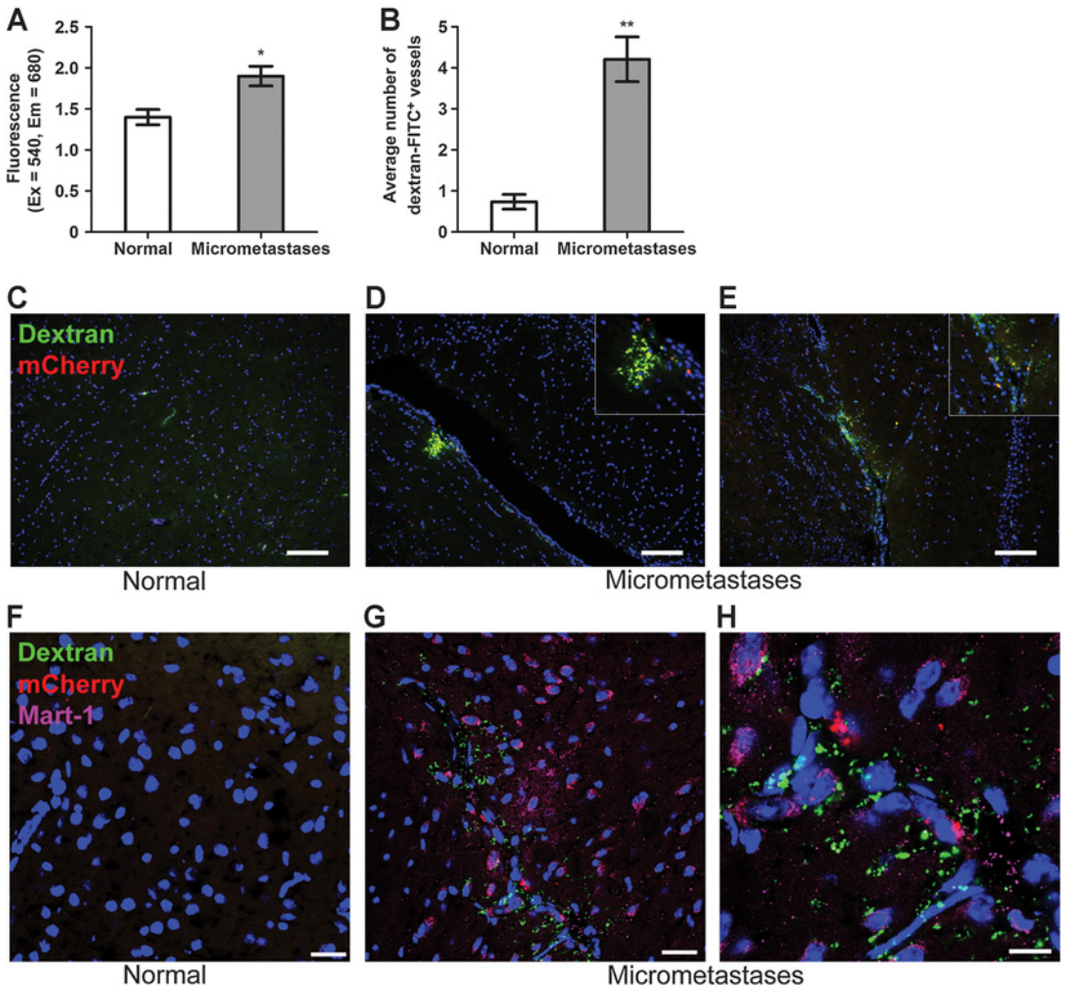

Figure 4.

Spontaneous formation of brain micrometastases is associated with increased vascular hyperpermeability. **A,** modified Miles assay quantification in normal brains ($n = 7$) or in brains with spontaneous micrometastases ($n = 15$), 1.5 months after tumor excision. Results shown are average of two independent experiments. Error bars, SEM. *, $P < 0.05$ (Student t test). **B,** quantification of FITC-Dextran–labeled blood vessels in brain sections of injected mice ($n = 3$, 92 fields) versus control mice ($n = 3$, 95 fields), 1.5 months after tumor excision. Error bars represent SEM of fields analyzed from each group. **, $P < 0.01$ (Student t test). **C–E,** representative images from multiple fields analyzed from control or injected mice as in **B**. Scale bars, 100 μm. **F–H,** Mart-1 (Magenta) staining depicting melanoma cells near FITC-Dextran–labeled leaky blood vessels. Representative of multiple fields analyzed from control or injected mice as above. In **F–G,** scale bars, 25 μm; **H,** scale bar, 10 μm.

mice injected with FITC-Dextran indicated that vessel permeability is correlated with the presence of disseminated melanoma cells around leaky blood vessels (Fig. 4C–H). These findings suggest that spontaneous brain micrometastases instigate breakdown of the blood–brain barrier.

Astrogliosis and neuroinflammation are instigated in incipient melanoma brain metastases

We next wanted to test the applicability of the model to characterize the formation of a hospitable metastatic niche. We previously demonstrated that astrocytes are recruited to experimental melanoma macrometastases in brain (21). Therefore, we set out to characterize the role of astrocytes in spontaneously occurring brain metastases. To that end, we analyzed astrocyte recruitment and activation by immunostaining with GFAP, a marker of activated astrocytes, in brain sections from mice injected subdermally with RMS cells. Analysis of the results confirmed that activated astrocytes surrounded macrometastatic lesions (Fig. 5A). Moreover, we analyzed the expression of GFAP in brain sections from patients and validated that astrogliosis is evident also in human melanoma brain metastasis (Fig. 5B). Importantly, analysis of staining in brains bearing micrometastases indicated that astrocyte recruitment and activation is an early event (Fig. 5C). Therefore, we next sought to determine when astrogliosis is first instigated during brain metastases formation. Analysis of brains bearing micrometastases (as determined by mCherry expression) indicated that the expression of GFAP is upregulated as early as 2–4 weeks after primary tumor removal (Fig. 5D), suggesting that astrogliosis precedes metastases formation.

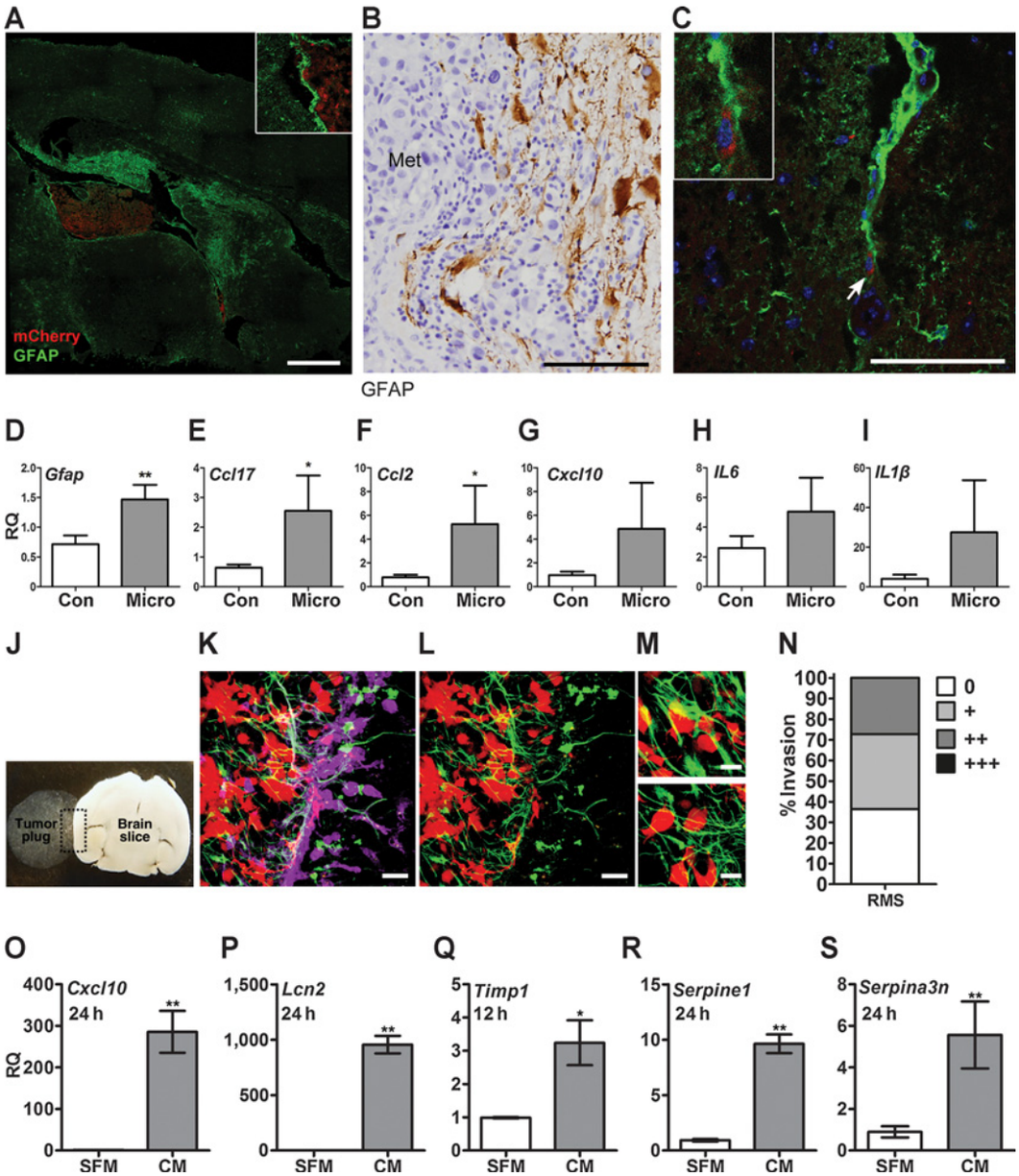

Figure 5.

Astrogliosis is induced in spontaneous melanoma brain metastasis. **A,** macrometastatic lesion in the ventricle. Immunostaining of astrocytes (GFAP, green) in tissue sections of spontaneous brain macrometastases (mCherry, red). Tiling of multiple images. Scale bar, 750 μm. **B,** representative image of tissue sections from human melanoma brain metastases; $n = 4$. Scale bar, 100 μm. Met, macrometastases. **C,** immunostaining, as in **A,** of tissue sections of spontaneous brain micrometastases. Scale bar, 75 μm. Images in **A** and **C** are representative of multiple fields analyzed from 3 mice in each cohort. **D,** qPCR analysis of GFAP expression in normal brains or in brains of injected mice, one month after tumor removal. **, $P < 0.01$ (Student's t-test). **E–I,** qPCR analyses of multiple chemokines and cytokines in total brains of injected mice. $n = 4$–6 mice in each group. Error bars, SEM. *, $P < 0.05$ (Student t test). Con, control mice; micro, injected mice bearing micrometastases. **J,** organotypic coculture brain slice model. Representative images were taken from the plug-brain slice interface (dashed rectangle). **K,** astrocytes (GFAP, green) and microglia (ILB4, violet) surround, infiltrate, and interact with invasive melanoma cells (mCherry). Scale bar, 50 μm. **L,** astrocyte protrusions penetrate the tumor plug and interact with melanoma cells. Scale bar, 50 μm. **M,** high power magnifications of fields from **L**. Scale bars, 20 μm. **N,** quantification of melanoma cell invasion into brain slices. Data represent percentage of cell invasion after 96-hour coculture ($n = 11$). **O–S,** qPCR analysis of the gliosis-related wound-healing gene signature in astrocytes following incubation with RMS-CM. SFM, serum-free medium. Representative results of three independent experiments. Error bars represent SD of technical repeats. **, $P < 0.01$; *, $P < 0.05$ (Student t test).

Neuroinflammation, manifested by upregulation of proinflammatory cytokines and chemokines is a feature of astrogliosis. To test whether this physiologic characteristic of astrogliosis is operative also in the metastatic niche, we analyzed the expression of multiple proinflammatory mediators in brains of mice bearing micrometastases, as above. Analysis of the expression results

revealed upregulation in known proinflammatory cytokines and chemokines, including CCL17, CCL2, CXCL10, IL6, and IL-1β (Fig. 5E–I), suggesting that instigation of neuroinflammation, associated with astrogliosis, is an early event in the metastatic cascade.

We previously demonstrated that astrocytes facilitate the invasiveness of brain-tropic human melanoma cells *in vitro* (21). The functional role of astrocytes in facilitating the invasiveness of melanoma cells was further supported in an organotypic 3D intact brain slices cocultured with a tumor plug containing melanoma cells (Fig. 5J). Analysis of brain slices by immunostaining indicated that activated astrocytes and microglia are recruited to the tumor–brain interface (Fig. 5K–N). Seeking to obtain functional evidence that astrogliosis could be induced by paracrine signaling from disseminated melanoma cells, we tested whether conditioned medium (CM) from RMS cells could activate primary adult astrocytes that we had isolated from brains of normal mice. In addition to auditing the expression of *Gfap*, we analyzed the expression of an astrogliosis-related wound-healing gene signature, including *Cxcl10*, *Lcn-2*, *Timp-1*, *SerpinE1*, and *Serpina3n* (Fig. 5O–S). This gene signature was recently demonstrated to be operative during stroke and LPS-induced astrogliosis (30). Expression analysis of astrocytes incubated with melanoma cells CM indicated that secreted factors from melanoma cells could upregulate the astrogliosis-related wound-healing gene signature in normal astrocytes. These results suggest that the same molecular pathways that are induced during brain tissue damage and in neuroinflammation are operative also during brain metastases formation.

Astrocytes facilitate the initial growth of metastatic melanoma cells

In addition to invasiveness, persistence of disseminated tumor cells at a hostile microenvironment is a critical limiting step of metastasis. We therefore asked whether astrocytes affect the initial growth of disseminated melanoma cells. To that end, we established a 3D coculture system to model incipient micrometastases. When dispersed melanoma cells (as few as 25 cells) were seeded in the presence of primary astrocytes they were more proliferative than control melanoma cells (Fig. 6A–C), suggesting that astrocytes are functionally necessary for the initial growth of melanoma cells.

To further assess the functional importance of astrocytes to the initial growth of melanoma cells *in vivo*, we coinjected a limiting number of melanoma cells admixed with adult primary astrocytes to mice brains. Strikingly, melanoma cells coinjected with astrocytes gave rise to significantly (9-fold) larger brain lesions than RMS-only controls (Fig. 6D–F), implying that astrocytes play a central role in supporting the growth of melanoma cells in the brain. Moreover, quantification of reactive astrocytes *in vivo* by immunostaining demonstrated that larger brain lesions are characterized by increased GFAP expression in the brain, reflecting recruitment and activation of host astrocytes (Fig. 6G–I). This astrogliosis was specifically instigated by tumor cells rather than by the tissue damage caused by intracranial injection, as intracranial injection of serum-free medium (SFM) to control mice did not induce astrogliosis at the indicated timepoint (Fig. 6I). To get molecular insight on the effect of the brain microenvironment on brain-metastasizing melanoma cells, we established a variant of brain-tropic melanoma cells (BT-RMS) by isolating tumor cells from brain macrometastases and reinjecting them to mice. Analysis of the ensuing brain metastasis after two rounds of selection revealed that the brain-tropic variants exhibited an increased incidence of brain metastasis and a shortened timeline from subdermal injection to the formation of spontaneous brain metastasis (Supplementary Fig. S7). Moreover, analysis of known signaling pathways indicated that the MAPK pathway was activated in brain-tropic melanoma cells as compared with the parental tumor cells (Fig. 6J and K). Interestingly, the PI3K pathway was also mildly activated (Supplementary Fig. S7). These results indicate that the MAPK pathway is activated by the brain microenvironment. Importantly, *in vitro* experiments, in which melanoma cells were incubated with secreted factors of activated astrocytes, revealed that astrocytes induce MAPK activation in RMS melanoma cells (Fig. 6L and M and Supplementary Fig. S7). These results imply that the *in vivo* activation of this pathway in brain-tropic melanoma cells is mediated, at least partially, by astrocytes. Thus, astrocytes support the growth of melanoma cells and activate signaling pathways associated with enhanced proliferation.

Finally, we analyzed the expression of the gliosis wound-healing gene signature in brains of mice coinjected with astrocytes as compared with brains of mice injected with melanoma cells only (Fig. 6N–R). Expression results revealed upregulation of genes known to be associated with astrogliosis. Notably, the upregulation of most genes was significant even when analyzed in total brain, containing multiple other cells in addition to activated astrocytes. These results functionally implicate the induction of astrogliosis and a wound-healing program in facilitating metastatic colonization and the initial growth of melanoma cells.

Taken together, utilizing a model of spontaneous melanoma brain metastasis, combined with molecular detection of micrometastases, we show that metastatic melanoma cells instigate blood vessel hyperpermeability, recruitment, and activation of astrocytes accompanied by induction of neuroinflammation, and that activated astrocytes functionally facilitate early metastatic growth (Fig. 7).

Discussion

Reciprocal interactions of metastasizing tumor cells with stromal cells in secondary sites are a key factor throughout the metastatic cascade (3). Here we show that incipient melanoma brain metastases instigate astrogliosis and neuroinflammation, which precede the formation of macrometastases.

Utilizing a model of spontaneous brain metastasis in immunocompetent mice, we demonstrate the initial changes in the brain metastatic niche. Early changes in the brain microenvironment included breakdown of the blood–brain barrier, recruitment of astrocytes, and instigation of proinflammatory mediators and a wound-healing gene signature that were associated with enhanced growth of melanoma cells in brain.

Reproducible models of brain metastasis that recapitulate the multistep process of metastases have been a major challenge for several decades (11, 31, 32). We have established a clinically relevant murine model of spontaneous melanoma brain metastasis in immunocompetent mice that provides a unique platform to study the pathophysiology of brain metastasis. The brain metastatic spread and histopathologic features of brain metastases in this model are comparable with the human disease (27), further supporting its clinical relevance. Notably, the RMS tumor

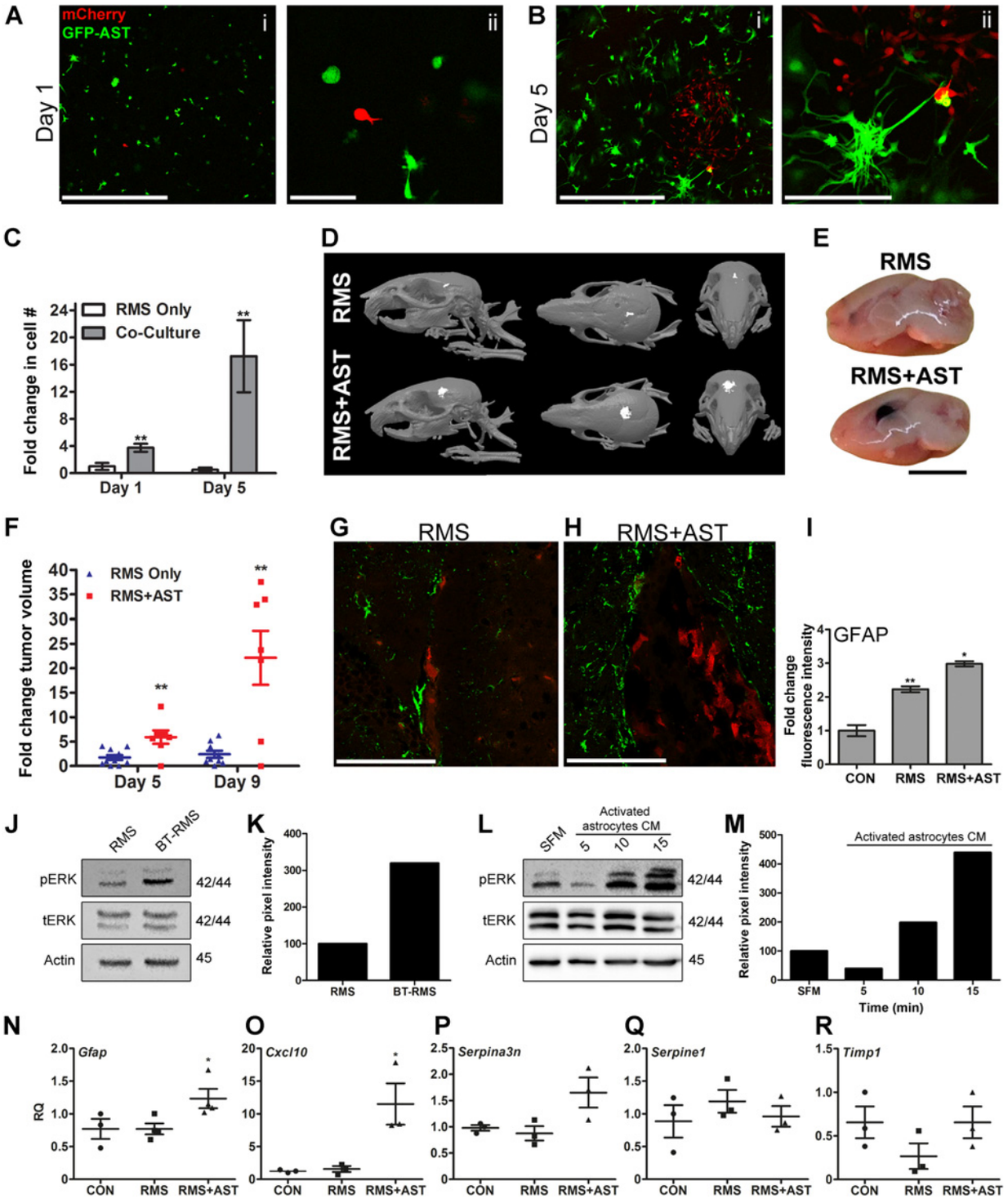

Figure 6.

Astrocytes functionally facilitate melanoma brain metastasis. **A** and **B,** representative images from 3D cocultures in day 1 and day 5. Red, melanoma cells; green, GFP-expressing astrocytes. ii, magnification of image shown in i. Scale bars in **A, i,** 750 μm; scale bar in **A, ii,** 100 μm; in **B, ii,** 250 μm. **C,** quantification of RMS cell number after 3D coculture with adult primary astrocytes. Representative results of two independent experiments. Experiments were run in duplicate and total of 7 fields/group were analyzed. Error bars, SEM. **, $P < 0.01$ (Student t test). **D,** representative CT images of brain tumors 5 and 9 days after intracranial inoculation of melanoma cells alone (RMS) or with astrocytes (RMS+AST); lateral (left), superior (middle), and frontal (right) views. **E,** gross anatomical view of the melanotic tumor lesions in RMS (top) or RMS coinjected with astrocytes (bottom). Scale bar, 5 mm. (*Continued on the following page.*)

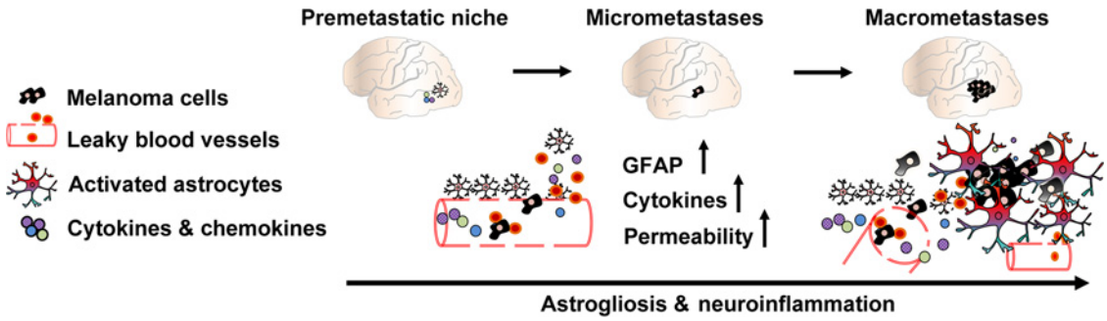

Figure 7.
Incipient melanoma brain metastases instigate blood vessel hyperpermeability, astrogliosis, and neuroinflammation.

cells used in this model were not selected for brain tropism by repeated injections, and thus represent authentic brain metastasis of cutaneous cells.

We characterized the temporal and pathologic progression of micro- and macrometastases formation and established a system for quantitative detection of brain metastatic load. We have established molecular and intravital methodologies to diagnose micrometastases and quantitatively determine brain metastatic burden (qPCR of melanoma transcripts in brains, CSF analysis).

The presence of tumor cells in CSF was previously reported to be associated with advanced disease: cytologic and molecular analysis detected melanoma cells in CSF from stage IV melanoma patients with brain metastases (33). Here we demonstrate that CSF can be utilized to detect melanoma-derived transcripts in exosomes, rather than in tumor cells seeded in the CSF, thus implicating this analysis in early diagnosis and monitoring of occult micrometastases.

Melanoma brain metastases instigate astrogliosis and neuroinflammation

Activated astrocytes were shown to be recruited to brain metastases (2). Moreover, we previously showed that paracrine signaling from brain-metastasizing melanoma cells contributes to reprogramming and activation of astrocytes *in vitro* (21). Here we show *in vivo* that activation of astrocytes and upregulation of a gene signature associated with inflammation and immune cell recruitment (e.g., CCL2, CXCL10, CCL17), are instigated in the brain metastatic niche before the formation of brain macrometastases. Neuroinflammation is a prominent characteristic of astrogliosis, which includes release of proinflammatory cytokines and chemokines, increased blood–brain barrier permeability, and leukocyte infiltration (34, 35). Sustained inflammation is present in both acute CNS injury and in chronic neurodegenerative disorders, and astrocytes are major players in neuroinflammation (36), but its role in facilitating brain metastases formation is largely unknown.

In addition to upregulation of a proinflammatory gene signature in astrocytes, we show that a gene signature associated with stroke and LPS-induced brain tissue damage (30) is instigated in astrocytes by brain-metastasizing melanoma cells *in vitro* as well as *in vivo*. Functionally, upregulation of gliosis genes *in vivo* was associated with enhanced metastatic colonization when melanoma cells were coinjected with astrocytes. This gliosis-related wound-healing gene signature includes the chemokine CXCL10, a known chemoattractant for T cells expressed by astrocytes during neuroinflammation associated with chronic inflammatory diseases in the CNS (37). Thus, our findings suggest that astrogliosis and neuroinflammation, physiologically instigated as a response of astrocytes to overcome brain tissue damage, are hijacked by brain-metastasizing tumor cells to support their growth.

Astrocytes facilitate the initial growth of metastatic melanoma cells

Survival and proliferation of disseminated cells in distant organs is a crucial junction in metastatic colonization. Astrocytes were previously shown to protect melanoma cells from chemotherapy via the endothelin–endothelin receptor signaling axis (38–40), and by direct contact through establishment of functional gap junctions via connexin 43 (41, 42). However, the role of astrocytes in facilitating the primary growth of brain-metastasizing melanoma cells is unknown. By seeding limiting numbers of melanoma cells and astrocytes in 3D cocultures, as well as in brains, we show, for the first time to the best of our knowledge, that astrocytes are functionally important in supporting the initial growth of metastatic melanoma cells. Molecular analysis

(*Continued.*) **F,** quantification of tumor volume described in **D**. Results were normalized to control. Representative results of two different cohorts analyzed; $n = 16$ in each. Error bars, SEM. **, $P < 0.01$. **G** and **H,** representative immunostaining pictures of astrocytes (GFAP, green) around tumor lesion (mCherry, red) in brains injected with RMS only (left) or in coinjected brains (right). Scale bars, 100 μm. **I,** quantification of total brain GFAP immunostaining in RMS only or in coinjected mice, compared with normal mice injected with SFM as control (CON). $n = 3$ in each group. Fifteen serial sections per mouse in CON, RMS, and RMS+AST from different brain regions were analyzed. A total of 37, 47, and 27 fields per group were quantified, respectively. Error bars, SEM. **, $P < 0.01$; *, $P < 0.05$. **J–M,** the MAPK signaling pathway is activated in BT-RMS cells. **J,** RMS or BT-RMS cells were incubated in SFM for 48 hours. pERK activation was analyzed by Western blot analysis. **K,** quantification of band intensity shown in **J**. Results were normalized to total ERK (tERK) and to RMS. **L,** the MAPK signaling pathway is activated in melanoma cells by astrocytes. Western blot analysis of RMS cells at different time points following incubation with activated astrocytes CM. **M,** quantification of band intensity shown in **L**; results were normalized to tERK and to SFM. **J–M** are representative of two independent experiments. **N–R,** qPCR of gliosis genes in total brain. Results were normalized to *Hprt*. $n = 3$ mice in each group. Error bars, SEM. *, $P < 0.05$.

of signaling pathways activated in brain-tropic melanoma cells (BT-RMS) suggested that this astrocyte-facilitated growth enhancement is mediated by activation of the MAPK signaling pathway in brain-metastasizing tumor cells.

Interestingly, the gliosis-related gene signature activated in astrocytes included SERPINs, recently shown to be involved in protection of brain-infiltrating cancer cells from FasL-mediated apoptosis (22). The study by Valiente and colleagues (22) demonstrated that secretion of SERPINs from tumor cells rescues them from astrocyte-mediated apoptosis. Our findings expand these observations and suggest that melanoma cells directly induce the expression of SERPINs in activated astrocytes, thus reprogramming astrocytes from growth inhibitory to growth promoting.

Importantly, we show that astrocyte activation is an early event, which occurs even before the formation of overt macrometastases. This implies that systemic or paracrine factors derived from circulating and/or disseminated tumor cells induce the formation of a hospitable metastatic niche in the brain. This observation is supported by our findings that melanoma cells can reprogram normal astrocytes to express GFAP and astrogliosis-related genes. Furthermore, our findings of melanoma-derived transcripts in exosomes also suggest that exosomes may be operative in the paracrine crosstalk between melanoma cells and astrocytes (4). Tumor cell-derived transcripts in exosomes were recently reported to support the formation of a premetastatic niche (43–45). Thus, astrocyte activation and reprogramming may be at least partially mediated by systemic signaling via exosomes.

Implications for preclinical studies

The development of targeted therapeutics (e.g., BRAF inhibitors and MEK inhibitors; ref. 46) and immune checkpoint blockade therapies has dramatically changed the landscape of melanoma treatment in recent years, making the immune system a central therapeutic target. The way forward in harnessing these new therapeutic options to provide survival benefit to patients is by understanding immune responses in the tumor microenvironment and investigating novel drug combinations (47). Importantly, Ret-melanoma cells are immunogenic, and induce the formation of TRP-2–specific T cells, which accumulate in the bone marrow and in tumors (48). Such T cells, specific for intrinsic melanoma antigens are also a feature of human melanoma, and are found in patients' blood (49). However, similar to human disease, immune modulation in the Ret-melanoma model results in immunosuppression; tumors are infiltrated with MDSCs that block antitumor T-cell activity and Tregs (50). Thus, our model may provide a clinically relevant platform to investigate combination therapeutics and to assess their effect on brain metastasis in an immunocompetent host. Moreover, we show that brain micrometastases are associated with vascular hyperpermeability, and with the presence of disseminated melanoma cells in proximity to leaky blood vessels. These findings will facilitate testing of therapeutics at early stages, as vascular leakiness was previously demonstrated to enable drug delivery (28). Application of these findings in human disease will enable the combination of intravital early diagnostics of brain metastasis with preventive therapeutics, which may be the key to limiting metastasis.

In summary, we have established and characterized a preclinical model of brain metastasis and utilized it to characterize the earliest changes in the brain metastatic niche. Molecular understanding of metastasis at its onset will enable the design of novel therapeutic approaches that may prevent brain metastatic relapse.

Disclosure of Potential Conflicts of Interest

No potential conflicts of interest were disclosed.

Authors' Contributions

Conception and design: H. Schwartz, K. Müller-Decker, R. Satchi-Fainaro, T. Pukrop, N. Erez

Development of methodology: H. Schwartz, E. Blacher, K. Müller-Decker, R. Satchi-Fainaro, N. Erez

Acquisition of data (provided animals, acquired and managed patients, provided facilities, etc.): H. Schwartz, E. Blacher, N. Livneh, L. Abramovitz, D. Ben-Shushan, R. Blazquez, A. Barrantes-Freer, M. Müller, K. Müller-Decker, R. Stein, R. Satchi-Fainaro, V. Umansky, T. Pukrop

Analysis and interpretation of data (e.g., statistical analysis, biostatistics, computational analysis): H. Schwartz, E. Blacher, M. Amer, N. Livneh, R. Blazquez, A. Barrantes-Freer, G. Tsarfaty, R. Satchi-Fainaro, T. Pukrop, N. Erez

Writing, review, and/or revision of the manuscript: H. Schwartz, E. Blacher, D. Ben-Shushan, A. Barrantes-Freer, R. Satchi-Fainaro, V. Umansky, T. Pukrop, N. Erez

Administrative, technical, or material support (i.e., reporting or organizing data, constructing databases): E. Blacher, A. Klein, S. Soffer

Study supervision: R. Stein, R. Satchi-Fainaro, N. Erez

Acknowledgments

The authors thank Dr. Pablo Blinder and Dr. Limor Broday for granting access to their facilities, Irena Shur and the Sackler School of Medicine Interdepartmental Core Facility (SICF) for help with imaging, FACS and PCR analyses, Prof. Ilan Hammel for his help with staining interpretations, Nasma Aqaqe for her help in FACS analyses, and Muhammad Yassin for his help with viral infections.

Grant Support

This research was supported by grants from The German–Israeli Cooperation in Cancer Research (MOST–DKFZ, CA-152 to N. Erez and K. Müller-Decker), from Worldwide Cancer Research (formerly known as the AICR; to N. Erez), and The Melanoma Research Alliance (the Saban Family Foundation–MRA Team Science Award to N. Erez and R. Satchi-Fainaro).

The costs of publication of this article were defrayed in part by the payment of page charges. This article must therefore be hereby marked *advertisement* in accordance with 18 U.S.C. Section 1734 solely to indicate this fact.

Received February 17, 2016; revised April 20, 2016; accepted May 2, 2016; published OnlineFirst June 3, 2016.

References

1. Nayak L, Lee EQ, Wen PY. Epidemiology of brain metastases. Curr Oncol Rep 2012;14:48–54.
2. Langley RR, Fidler IJ. The biology of brain metastasis. Clin Chem 2013;59:180–9.
3. Joyce JA, Pollard JW. Microenvironmental regulation of metastasis. Nat Rev Cancer 2009;9:239–52.
4. Peinado H, Lavotshkin S, Lyden D. The secreted factors responsible for pre-metastatic niche formation: old sayings and new thoughts. Semin Cancer Biol 2011;21:139–46.
5. Eichler AF, Chung E, Kodack DP, Loeffler JS, Fukumura D, Jain RK. The biology of brain metastases-translation to new therapies. Nat Rev Clin Oncol 2011;8:344–56.

6. Cruz-Munoz W, Man S, Xu P, Kerbel RS. Development of a preclinical model of spontaneous human melanoma central nervous system metastasis. Cancer Res 2008;68:4500–5.
7. Izraely S, Sagi-Assif O, Klein A, Meshel T, Tsarfaty G, Pasmanik-Chor M, et al. The metastatic microenvironment: brain-residing melanoma metastasis and dormant micrometastasis. Int J Cancer 2012;131:1071–82.
8. Ackermann J, Frutschi M, Kaloulis K, McKee T, Trumpp A, Beermann F. Metastasizing melanoma formation caused by expression of activated N-RasQ61K on an INK4a-deficient background. Cancer Res 2005;65: 4005–11.
9. Lindsay CR, Lawn S, Campbell AD, Faller WJ, Rambow F, Mort RL, et al. P-Rex1 is required for efficient melanoblast migration and melanoma metastasis. Nat Commun 2011;2:555.
10. Dankort D, Curley DP, Cartlidge RA, Nelson B, Karnezis AN, Damsky WE Jr, et al. Braf(V600E) cooperates with Pten loss to induce metastatic melanoma. Nat Genet 2009;41:544–52.
11. Daphu I, Sundstrom T, Horn S, Huszthy PC, Niclou SP, Sakariassen PO, et al. In vivo animal models for studying brain metastasis: value and limitations. Clin Exp Metastasis 2013;30:695–710.
12. Kato M, Takahashi M, Akhand AA, Liu W, Dai Y, Shimizu S, et al. Transgenic mouse model for skin malignant melanoma. Oncogene 1998;17:1885–8.
13. Kuzu OF, Nguyen FD, Noory MA, Sharma A. Current state of animal (Mouse) modeling in melanoma research. Cancer Growth Metastasis 2015;8(Suppl 1):81–94.
14. Mulligan LM. RET revisited: expanding the oncogenic portfolio. Nat Rev Cancer 2014;14:173–86.
15. Ohshima Y, Yajima I, Takeda K, Iida M, Kumasaka M, Matsumoto Y, et al. c-RET molecule in malignant melanoma from oncogenic RET-carrying transgenic mice and human cell lines. PLoS One 2010;5:e10279.
16. Deutsch GB, Yost S, Deutsch MB, Lee JH, Foshag L, Barkhoudarian G, et al. Predictors of CNS disease in metastatic melanoma: desmoplastic subtype associated with higher risk. Oncology 2015;29:pii: 204997.
17. Abschuetz O, Osen W, Frank K, Kato M, Schadendorf D, Umansky V. T-cell mediated immune responses induced in ret transgenic mouse model of malignant melanoma. Cancers 2012;4:490–503.
18. Verkhratsky A, Parpura V. Astrogliopathology in neurological, neurodevelopmental and psychiatric disorders. Neurobiol Dis 2016;85:254–61.
19. Langley RR, Fan D, Guo L, Zhang C, Lin Q, Brantley EC, et al. Generation of an immortalized astrocyte cell line from H-2Kb-tsA58 mice to study the role of astrocytes in brain metastasis. Int J Oncol 2009;35:665–72.
20. Kamphuis W, Kooijman L, Orre M, Stassen O, Pekny M, Hol EM. GFAP and vimentin deficiency alters gene expression in astrocytes and microglia in wild-type mice and changes the transcriptional response of reactive glia in mouse model for Alzheimer's disease. Glia 2015;63:1036–56.
21. Klein A, Schwartz H, Sagi-Assif O, Meshel T, Izraely S, Ben Menachem S, et al. Astrocytes facilitate melanoma brain metastasis via secretion of IL-23. J Pathol 2015;236:116–27.
22. Valiente M, Obenauf AC, Jin X, Chen Q, Zhang XH, Lee DJ, et al. Serpins promote cancer cell survival and vascular co-option in brain metastasis. Cell 2014;156:1002–16.
23. Xing F, Kobayashi A, Okuda H, Watabe M, Pai SK, Pandey PR, et al. Reactive astrocytes promote the metastatic growth of breast cancer stem-like cells by activating Notch signalling in brain. EMBO Mol Med 2013;5:384–96.
24. Liu L, Duff K. A technique for serial collection of cerebrospinal fluid from the cisterna magna in mouse. J Vis Exp 2008;e960. doi:10.3791/960.
25. Zhao F, Falk C, Osen W, Kato M, Schadendorf D, Umansky V. Activation of p38 mitogen-activated protein kinase drives dendritic cells to become tolerogenic in ret transgenic mice spontaneously developing melanoma. Clin Cancer Res 2009;15:4382–90.
26. Cornil I, Man S, Fernandez B, Kerbel RS. Enhanced tumorigenicity, melanogenesis, and metastases of a human malignant melanoma after subdermal implantation in nude mice. J Natl Cancer Inst 1989;81:938–44.
27. Clarke JL, Perez HR, Jacks LM, Panageas KS, Deangelis LM. Leptomeningeal metastases in the MRI era. Neurology 2010;74:1449–54.
28. Satchi-Fainaro R, Mamluk R, Wang L, Short SM, Nagy JA, Feng D, et al. Inhibition of vessel permeability by TNP-470 and its polymer conjugate, caplostatin. Cancer Cell 2005;7:251–61.
29. Zhang RD, Price JE, Fujimaki T, Bucana CD, Fidler IJ. Differential permeability of the blood-brain barrier in experimental brain metastases produced by human neoplasms implanted into nude mice. Am J Pathol 1992;141:1115–24.
30. Zamanian JL, Xu L, Foo LC, Nouri N, Zhou L, Giffard RG, et al. Genomic analysis of reactive astrogliosis. J Neurosci 2012;32:6391–410.
31. Alterman AL, Stackpole CW. B16 melanoma spontaneous brain metastasis: occurrence and development within leptomeninges blood vessels. Clin Exp Metastasis 1989;7:15–23.
32. Cruz-Munoz W, Kerbel RS. Preclinical approaches to study the biology and treatment of brain metastases. Semin Cancer Biol 2011;21: 123–30.
33. Hoon DS, Kuo CT, Wascher RA, Fournier P, Wang HJ, O'Day SJ. Molecular detection of metastatic melanoma cells in cerebrospinal fluid in melanoma patients. J Invest Dermatol 2001;117:375–8.
34. Downes CE, Crack PJ. Neural injury following stroke: are Toll-like receptors the link between the immune system and the CNS? Br J Pharmacol 2010;160:1872–88.
35. Van Eldik LJ, Thompson WL, Ralay Ranaivo H, Behanna HA, Martin Watterson D. Glia proinflammatory cytokine upregulation as a therapeutic target for neurodegenerative diseases: function-based and target-based discovery approaches. Int Rev Neurobiol 2007;82:277–96.
36. Marchetti B, Abbracchio MP. To be or not to be (inflamed)–is that the question in anti-inflammatory drug therapy of neurodegenerative disorders? Trends Pharmacol Sci 2005;26:517–25.
37. Ubogu EE, Cossoy MB, Ransohoff RM. The expression and function of chemokines involved in CNS inflammation. Trends Pharmacol Sci 2006;27:48–55.
38. Fidler IJ. The role of the organ microenvironment in brain metastasis. Semin Cancer Biol 2011;21:107–12.
39. Kim SJ, Kim JS, Park ES, Lee JS, Lin Q, Langley RR, et al. Astrocytes upregulate survival genes in tumor cells and induce protection from chemotherapy. Neoplasia 2011;13:286–98.
40. Kim SW, Choi HJ, Lee HJ, He J, Wu Q, Langley RR, et al. Role of the endothelin axis in astrocyte- and endothelial cell-mediated chemoprotection of cancer cells. Neuro Oncol 2014;16:1585–98.
41. Kamiya T, Mobley AK, Bar-Eli M. Crossing the junction in the gap of melanoma brain metastasis. Pigment Cell Melanoma Res 2013;26:435–7.
42. Lin Q, Balasubramanian K, Fan D, Kim SJ, Guo L, Wang H, et al. Reactive astrocytes protect melanoma cells from chemotherapy by sequestering intracellular calcium through gap junction communication channels. Neoplasia 2010;12:748–54.
43. Costa-Silva B, Aiello NM, Ocean AJ, Singh S, Zhang H, Thakur BK, et al. Pancreatic cancer exosomes initiate pre-metastatic niche formation in the liver. Nat Cell Biol 2015;17:816–26.
44. Peinado H, Aleckovic M, Lavotshkin S, Matei I, Costa-Silva B, Moreno-Bueno G, et al. Melanoma exosomes educate bone marrow progenitor cells toward a pro-metastatic phenotype through MET. Nat Med 2012;18: 883–91.
45. Hoshino A, Costa-Silva B, Shen TL, Rodrigues G, Hashimoto A, Tesic Mark M, et al. Tumour exosome integrins determine organotropic metastasis. Nature 2015;527:329–35.
46. Michielin O, Hoeller C. Gaining momentum: new options and opportunities for the treatment of advanced melanoma. Cancer Treat Rev 2015;41: 660–70.
47. Sharma P, Allison JP. The future of immune checkpoint therapy. Science 2015;348:56–61.
48. Umansky V, Abschuetz O, Osen W, Ramacher M, Zhao F, Kato M, et al. Melanoma-specific memory T cells are functionally active in Ret transgenic mice without macroscopic tumors. Cancer Res 2008;68:9451–8.
49. Purwar R, Schlapbach C, Xiao S, Kang HS, Elyaman W, Jiang X, et al. Robust tumor immunity to melanoma mediated by interleukin-9-producing T cells. Nat Med 2012;18:1248–53.
50. Meyer C, Sevko A, Ramacher M, Bazhin AV, Falk CS, Osen W, et al. Chronic inflammation promotes myeloid-derived suppressor cell activation blocking antitumor immunity in transgenic mouse melanoma model. Proc Natl Acad Sci U S A 2011;108:17111–6.